Sea-Surface Floating Small Target Detection by Multifeature Detector Based on Isolation Forest

Shuwen Xu, *Member, IEEE*, Jianan Zhu, Junzheng Jiang, and Penglang Shui, *Senior Member, IEEE*

***Abstract*—In this article, a multifeature detector based on isolation forest (iForest) algorithm is developed to detect floating small targets in sea clutter. The conventional multifeature detector can only process three features or less. The proposed detector aims to break the limitation of feature dimensions' number of the existed feature-based detectors and to improve the detection performance. It transforms the detection of floating small target into an anomaly detection problem in a high-dimensional feature space, breaking the limitation of the number of features. First, a modified isolation forest is constructed from multiple features extracted from sea clutter. Meanwhile, the relative Doppler coefficient of variation is proposed and added into the feature library. Then, taking the average path length as detection statistic, the detection threshold is obtained by Monte-Carlo technique at the given false alarm probability. Finally, the final decision is made by comparing the path length calculated from the cell under test of radar returns with the detection threshold. Detection performances are evaluated based on twenty measured IPIX radar datasets. The experiment results show that the multifeature detector based on isolation forest can obtain a significant performance improvement and has lower computation cost compared with the existed detectors.**

***Index Terms*—Feature detection, floating small target detection, isolation forest algorithm, sea clutter.**

I. Introduction

THE detection of sea-surface floating small targets, such as floating ice, victims of aircraft crashes at sea, vent pipes, periscopes of the submarine, etc., has always been a difficult problem in the field of radar target detection. The difficulties of detecting floating small targets in sea clutter arise from the complex and varying characteristics of sea clutter, wider Doppler bandwidth, and smaller radar cross section (RCS) of weak target [1], [2]. However, the effective detection of such targets is of great significance for navigation safety, sea-surface rescue, and national defense security.

High resolution sea clutter, with large fluctuations and heavy tail, usually shows the non-Gaussian characteristics, which deviates from the Gaussian clutter. In recent years, the compound Gaussian model is used to characterize heavy-tailed sea clutter successfully. The K distribution with Gamma texture [3], the generalized Pareto distribution with inverse Gamma texture [4], [5] and the compound Gaussian distribution with inverse Gaussian texture (CG-IG) [6] have been used to model sea clutter under different environment and radar parameters. All sea clutter models have their optimal detectors or near-optimal detectors, such as the optimum K detector (OKD) for the K-distribution clutter [7], the generalized likelihood ratio test linear-threshold detector (GLRT-LTD) for generalized Pareto clutter [5] and the generalized likelihood ratio test with IG texture (GLRT-IG) detector for CG-IG clutter [6], and they all distinguish target from sea clutter by energy difference. However, weaker energy of target and lower radial velocity between target and radar of floating small target make the energy-based detectors unable to fully exert their advantages. In order to accumulate more energy in different frequency subbands, the modified adaptive coherent detectors [8], [9] have been applied to solve this problem. Nevertheless, these detectors require that potential targets must keep a constant radial velocity during the integration time and the relatively high signal-to-clutter ratio (SCR). Naturally, these rigorous requirements limit their scalability of the practical application seriously, especially for the detection of floating small target.

For floating small targets, traditional detection methods, such as the constant false alarm rate (CFAR) class detectors or the adaptive class detectors, exhibit an unacceptable performance loss. In recent years, many detectors employed in target detection in sea clutter have been proposed, which are almost applicable for large warship targets, but not suitable for floating small targets. There are a few detectors designed for floating small target detection. First, some modified adaptive detectors were proposed, such as the block-adaptive clutter suppression and subband adaptive detectors [8], [9], which have been introduced above. Second, the nonlinear detectors based on fractal characters [10] change the approach of establishing the sea clutter model, but the single detection feature fails to make full use of the return information and has not obtained satisfactory detection performance. In addition, the neural-network-based detector [11], [12] is not suitable for practical application due to higher computational complexity, the lack of target training

Manuscript received August 2, 2020; revised October 3, 2020; accepted October 16, 2020. Date of publication October 22, 2020; date of current version January 6, 2021. This work was supported in part by the National Natural Science Foundation of China under Grant 61871303 and Grant 62071346, in part by the foundation of National Key Laboratory of Electromagnetic Environment under Grant 6142403180204, and in part by the Foreign Scholars in University Research and Teaching Programs (the 111 Project) under Grant B18039. *(Corresponding author: Shuwen Xu.)*

Shuwen Xu is with the National Lab of Radar Signal Processing, Xidian University, Xi'an 710071, China, and also with the Mcmaster University, Hamilton, ON L8S4L8, Canada (e-mail: swxu@mail.xidian.edu.cn).

Jianan Zhu is with the Signal processing Department, Nanjing Research Institute of Electronics Technology, Nanjing L8S4L8, China (e-mail: pig_zjn@163.com).

Junzheng Jiang is with the School of Information and Communication, Guilin University of Electronic Technology, Guilin 541004, China (e-mail: jzjiang@guet.edu.cn).

Penglang Shui is with the National Lab of Radar Signal Processing, Xidian University, Xi'an 710071, China (e-mail: plshui@xidian.edu.cn).

Digital Object Identifier 10.1109/JSTARS.2020.3033063

samples and the difficulty of controlling the false alarm probability (PFA). Third, the detectors based on multiple features are a class of novel and effective methods to detect floating small targets. Via the long autoregressive model, the parameters of Doppler power spectra (DPS) of time series are mapped into Riemannian manifold [13], and then the detection is accomplished by Riemannian geometry method. Trifeature-based detectors, including amplitude and Doppler three features [14], polarization information three features [15], and three time-frequency (TF) features [16], achieve fairly good detection performance for floating small targets detection. However, the fast convexhull learning algorithm can only use three detection features at most, because PFA of convexhull is hard to control precisely in high-dimensional space (feature dimension is larger than 3). In addition, the detection must be processed as fast as possible to get the result in practical application. Since the high computational complexity of convexhull-class detectors makes it difficult to adapt to the fast-changing sea scene, it is also a disadvantage of the abovementioned trifeature-based detectors. Moreover, although the support vector machine (SVM)-based detector [17] obtains good detection performance, applying the measured data to model training and testing is a typical two-class classification strategy. Two-class classification model, such as the SVM or other models requiring target samples for training, is one-sided and unavailable in practical detection for the lack of target samples and the variety of targets. Thus, the two-class classification model is not suitable for radar target detection up to now. In addition, the principal component analysis (PCA)-based detector [18] makes the training samples and testing samples with different detection models, so it has a great deviation from radar target detection and cannot be well used.

Data anomaly detection, as one of the important tasks of data mining [19], is the process of finding instances in a dataset which are different from the majority of the data. Anomaly detection has been applied in a variety of application fields, such as fraud detection in finance, fault diagnosis in mechanics, and intrusion detection in network security. For floating small target detection in sea-surface, anomaly detection algorithms only need easily-obtained sea clutter samples for training detection models, which is more suitable for the problem. Local outlier factor (LOF)[20], [21], one-class SVM (OCSVM) [22], [23], robust covariance [24], and isolation forest (iForest) algorithm [25], [26] are the representative anomaly detection algorithms. Inspired by the convexhull-class detector, this article proposes a multifeature detector based on iForest algorithm. It overcomes the shortcomings that convexhull cannot make full use of multiple features and the defects of local effective detection algorithm guided by target samples. This detector can arbitrarily utilize a variety of detection features and effectively detect small targets in high-dimensional space. In addition, the relative Doppler coefficient of variance (RCV) is introduced and utilized in our proposed detector. Because of the advantage of the isolation forest algorithm with linear computational complexity, the proposed detector has a much lower computational complexity compared with the convexhull-class detectors.

The remainder of this article is organized as follows. In Section II, the detection problem of floating small targets in sea clutter and the measured datasets are described. Seven detection features are briefly introduced in Section III and an additional detection feature in the Doppler domain is proposed, together with multifeature detector based on isolation forest algorithm. Section IV gives the experimental results of the proposed detector and presents a comparison with several existing detectors. Finally, Section V concludes the article.

II. Detection Problem Description and the Measured IPIX Data

A. Formulation of Detection Problem

Assuming that marine surveillance radar transmits a train of coherent pulses at a beam position to search floating small targets. Here, we can formulate the detection problem of sea-surface floating small targets as the following binary hypothesis test:

$$\begin{cases} \mathrm{H}_0 : \begin{cases} x(n) = c(n), n = 1, 2, \ldots, N \\ x_k(n) = c_k(n), k = 1, 2, \ldots, K \end{cases} \\ \mathrm{H}_1 : \begin{cases} x(n) = s(n) + c(n), n = 1, 2, \ldots, N \\ x_k(n) = c_k(n), k = 1, 2, \ldots, K \end{cases} \end{cases} \tag{1}$$

where the null hypothesis H_0 denotes the absence of target in the cell under test (CUT), and the alternative hypothesis H_1 denotes the presentation of target in the CUT. $x(n)$ is the received time series in the CUT and $x_k(n)$ is the reference cells (RCs), which are a number of range cells selected around the CUT to estimate the sea clutter characteristics of the CUT. $s(n)$ is the returns of floating small target, $c(n)$ and $c_k(n)$ are sea clutter plus noise at the CUT and the RCs, respectively. N is the length of time series and K is the number of the RCs.

The RCs are several range units selected in the range dimension to estimate the sea clutter characteristics.

B. Measured Datasets

Twenty IPIX datasets [27] listed in Table I are always used to evaluate the performance of floating small target detectors. The range cell where the target is located is labeled as the primary cell. Around the primary cell, several range cells affected by the target are labeled as guard cells, which aren't used in the detection procedure. The IPIX radar operates on X-band, and works at dwell mode and at a low grazing angle (about 0.33°). Its pulse repetition frequency (PRF) is 1 kHz and radar returns include the echoes from HH, HV, VH, and VV polarizations. The top ten groups in Table I were collected in Nova, Scotia, the east coast of Canada, in 1993. Each group consists of 2^{17} pulses (dwell time is about 131 s) and 14 range cells. Radar was mounted on a 30-m high cliff and illuminated on the surface of the Atlantic Ocean. The cooperative target is a floating plastic ball wrapped by aluminum wire and the radius of which is approximately 0.5 m. The last ten groups in Table I were collected in Grimsby, Ontario, Canada, in 1998. Each group consists of 6×10^4 pulses (dwell time is 60 s) and 28 range cells. Radar erection height is 20 m and the cooperative target is a floating boat. The range resolution of the 18th and 19th dataset are 15 and 9 m, respectively. And the remaining datasets' range resolution

TABLE I
DESCRIPTION OF 20 DATASETS OF IPIX DATABASE

Data Label	File Name	Primary Cell	Guard Cell
1	19931107_135603_starea17	9	8,10,11
2	19931108_220902_starea26	7	6,8
3	19931109_191449_starea30	7	6,8
4	19931109_202217_starea31	7	6,8,9
5	19931110_001635_starea40	7	5,6,8
6	19931111_163625_starea54	8	7,9,10
7	19931118_023604_stareC0000280	8	7,9,10
8	19931118_162155_stareC0000310	7	6,8,9
9	19931118_162658_stareC0000311	7	6,8,9
10	19931118_174259_stareC0000320	7	6,8,9
11	19980204_202225_ANTSTEP	24	23,25,26
12	19980204_202525_ANTSTEP	7	6,8,9
13	19980204_163113_ANTSTEP	24	23,25,26
14	19980205_171437_ANTSTEP	7	6,8,9
15	19980205_180558_ANTSTEP	7	6,8,9
16	19980212_195704_ANTSTEP	7	6,8,9
17	19980223_164055_ANTSTEP	31	30,32,33
18	19980223_173317_ANTSTEP	32	31,33,34
19	19980223_173950_ANTSTEP	29	28,3034
20	19980304_184537_ANTSTEP	21	20,22

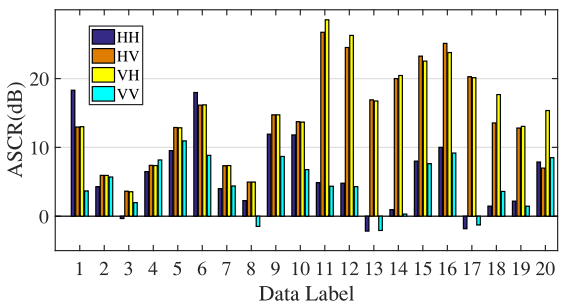

Fig. 1. Average SCRs of 20 datasets in the primary cells at four polarizations.

is 30 m. The numbers of CUT and guard cells are illustrated in Table I and the remaining cells are RCs.

The average SCRs (ASCR) at CUT are analyzed in four polarizations. The returns between CUT and RCs are assumed to be statistically independent and $\bar{P}_c$ is the clutter power estimated from RCs. The ASCR of each dataset can be calculated by

$$\mathrm{ASCR} = 10\log_{10}\frac{\frac{1}{N}\sum_{n=1}^{N}|x(n)|^2 - \bar{P}_c}{\bar{P}_c}. \tag{2}$$

Fig. 1 has plotted ASCRs of the twenty datasets. It is found that ASCRs vary with the dataset and polarization, which are also influenced by sea state and characteristic of test targets. The twenty datasets could well measure the detection performance of floating small target detector.

III. FEATURE EXTRACTION AND THE MULTIFEATURE DETECTOR BASED ON IFOREST

The single feature detector, such as the normalized Hurst exponent (NHE) [10], usually cannot obtain a satisfactory detection result because the returns' information is not well utilized. It is a feasible approach to employ multiple features to improve detection performance [16]. In radar target detection, the separation capacity differences of each feature between the target and sea clutter are very difficult to evaluate, because this depends on many factors, such as the target type and sea clutter condition, etc. The target is unknown, and there are many kinds of targets in the practical application. What's more, the characteristics of the target vary with the angle of the radar line of sight. Therefore, robust detection can only be achieved by quickly combining multiple features that have the ability to distinguish target and sea clutter. Multiple features can reflect the differences between sea clutter and target from different perspectives as much as possible. In this section, seven existing detection features for floating small target detection are reviewed briefly and the RCV feature is proposed and described in detail. Then, a multifeature detector based on isolation forest (iForest) algorithm is proposed.

A. Description of Multiple Features

In this section, we introduce the eight features used in the proposed detector. These features can be divided into four groups.

1) *Time Domain Feature [the Relative Average Amplitude (RAA)]*

It is the most common method of the energy-based detector for radar target detection. Most of the recent radar systems employ the first-order and second-order statistics of radar returns. For specific target and clutter models, statistics according to the GLRT are designed. Here we use an easily available energy information as a detection feature. First of all, we assume that $\mathbf{x} = \{x(n)|n = 1, 2, \ldots, N\}$ is an N-length time series and comes from a range cell, and its average amplitude of every range cell is readily available by taking a mean operation on the $\mathbf{x}$. To reduce the impact caused by inhomogeneous sea clutter, a usual method is to take the ratio of the CUT's statistic to the RCs' statistic as the final detection feature. So the RAA is defined as

$$\mathrm{RAA}(\mathbf{x}) \equiv \frac{\bar{A}(\mathbf{x})}{\frac{1}{K}\sum_{k=1}^{K}\bar{A}(\mathbf{x}_k)} \tag{3}$$

where $\bar{A}(\mathbf{x})$ is the average amplitude of CUT, $\bar{A}(\mathbf{x}_k)$ denotes the kth average amplitude of RC, and K is the number of RC.

2) *Doppler Domain Feature [the Relative Doppler Peak High (RPH), the Relative Vector Entropy (RVE), and the RCV]*

Owing to the micro motion of plenty of sea-surface scatters, the Doppler amplitude spectrum of sea clutter shows a wide Doppler width. The lower radial velocity of small targets causes their Doppler spectrum peak to be overlapped by sea clutter's clutter region, which gives rise to a great performance loss of the Doppler-based detector. However, during long observation, the differences of Doppler domain will emerge between sea clutter and returns from targets. The Doppler amplitude spectrum of

$\mathbf{x}$ is acquired by

$$\mathbf{X}(f_d) = \frac{1}{\sqrt{N}}\left|\sum_{n=1}^{N} x(n)exp(-j2\pi f_d nTr)\right| \quad -\frac{1}{2T_r} \le f_d \le \frac{1}{2T_r} \tag{4}$$

where f_d denotes the Doppler frequency and T_r is the pulse repetition interval (PRI).

Like the moving target detection, the maximum amplitude value (peak high PH($\mathbf{x}$), see [14] for details) of Doppler spectrum's clutter bin shows the slow change of velocity of the target compared with sea clutter. The RPH is defined as

$$\mathrm{RPH}(\mathbf{x}) \equiv \frac{\mathrm{PH}(\mathbf{x})}{\frac{1}{K}\sum_{k=1}^{K}\mathrm{PH}(\mathbf{x}_k)}. \tag{5}$$

Furthermore, it is found that the Doppler amplitude spectrum of sea clutter only is more dispersed than that of target plus sea clutter. Thus, Shannon entropy could be applied to detect floating small target in sea clutter [28] and shown as follows [14]:

$$\mathrm{VE}(\mathbf{x}) \equiv -\sum_{f_d}\tilde{X}(f_d)\log\tilde{X}(f_d), \tilde{X}(f_d) = \frac{\mathbf{X}(f_d)}{\Sigma_{f_d}\mathbf{X}(f_d)} \tag{6}$$

where VE$(\cdot)$ denotes the vector entropy of the item and $\tilde{X}(f_d)$ is the normalized Doppler amplitude spectrum. Taking the VE($\mathbf{x}$) of reference cells into consideration, The RVE is defined as

$$\mathrm{RVE}(\mathbf{x}) \equiv \frac{\mathrm{VE}(\mathbf{x})}{\frac{1}{K}\sum_{k=1}^{K}\mathrm{VE}(\mathbf{x}_k)}. \tag{7}$$

RCV, a new feature, can be employed to measure the sharpness of the Doppler amplitude spectrum. The coefficient of variation has been already applied to image focusing of synthetic aperture radar (SAR) and measure the sharpness of the high resolution range profile (HRRP) peak for range spread target (RST) detection [29]. When small targets are located in a range cell, there are several peaks in the Doppler amplitude spectrum. Therefore, the RCV can distinguish the target from sea clutter from the sharpness of Doppler spectrum peak. The coefficient of variation (CV) of the Doppler amplitude spectrum is calculated by

$$\mathrm{CV}(\mathbf{x}) = \frac{\sqrt{\frac{1}{N}\sum_{f_d}\left(\mathbf{X}(f_d) - \frac{1}{N}\sum_{f_d}\mathbf{X}(f_d)\right)^2}}{\frac{1}{N}\sum_{f_d}\mathbf{X}(f_d)}. \tag{8}$$

Therefore, the RCV of the Doppler spectrum is defined as

$$\mathrm{RCV}(\mathbf{x}) \equiv \frac{\mathrm{CV}(\mathbf{x})}{\frac{1}{K}\sum_{k=1}^{K}\mathrm{CV}(\mathbf{x}_k)} \tag{9}$$

where CV($\mathbf{x}$) and CV($\mathbf{x}_k$) are the CV of radar returns at the CUT and RCs, respectively. By comparing the three Doppler detection features in Fig. 2(b)–(d), it can be found that the proposed detection feature RCV has a smaller overlap region of sea clutter and returns with target, which means better potential detection performance.

3) *Fractal Dimension Domain [the Normalized Hurst Exponent of Fractal Feature]*

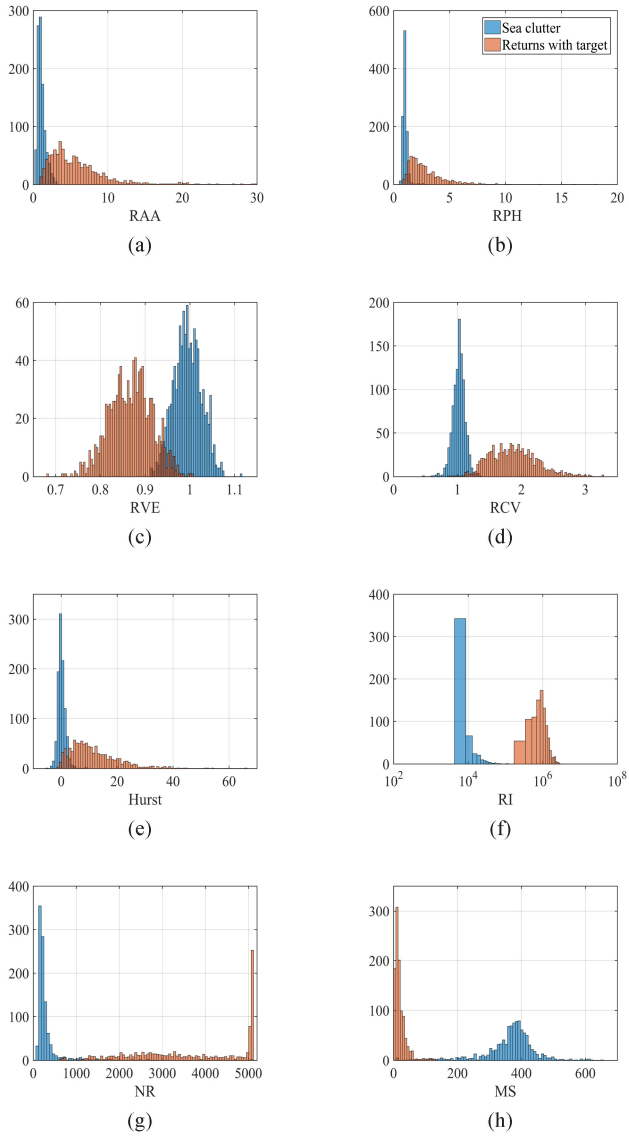

Fig. 2. Histogram contrast of (a) RAA, (b) RPH, (c) RVE, (d) RCV, (e) NHE, (f) RI, (g) NR, and (h) MS features between sea clutter's returns and target's returns on the 10th group dataset at HV polarization.

The fractal feature of sea clutter amplitude time series shows sea surface's self-similarity, which could reflect its roughness. In 1993, the fractal was first applied to the detection of floating small target [10]. Verified by measured IPIX datasets, the normalized Hurst exponent (NHE) of the fractal-based detector [10] gets a marked improvement for the problem.

The amplitude time series of sea clutter $\mathbf{x} = \{x(n)|n = 1, 2, \ldots, N\}$ is modeled as a random walk process [10]

$$F(m) = \left(\sum_{n=1}^{N-m}|x(n+m) - x(n)|^2\right)^{1/2}. \tag{10}$$

The region is from $m = 2^4$ to $m = 2^{12}$, (10) approximately satisfies the following equation:

$$F(m) \sim m^H \tag{11}$$

where H is the Hurst exponent of $\mathbf{x}$. The advantage of CUT's Hurst exponent normalized by mean and standard variance of RCs' Hurst exponent has been verified in [10]. We assume that $H_k, k = 1, 2, \ldots, K$ is the Hurst exponent of RCs. After acquiring the mean $\bar{\mu}$ and standard deviation σ of H_k, the normalized Hurst exponent (NHE) is defined as

$$\mathrm{NHE}(\mathbf{x}) \equiv \frac{H_c - \bar{\mu}}{\sigma} \tag{12}$$

where H_c is the Hurst exponent calculating from CUT.

4) *TF Domain Features [the Ridge Integration (RI), the Number of Connected Regions (NR), and the Maximum Size (MS) of Connected Regions]*

In a long observation time, the detection of floating small targets on the sea-surface can be considered as a problem of detecting nonlinear frequency modulation (FM) signals in sea clutter. Therefore, it is an effective way to include the detection features by TF analysis of the received radar returns and to extract the effective features from the TF images that are conducive to the detection of floating small targets. Here, we only give a brief overview of the TF features that have been derived in detail in [16] and apply these TF features to the subsequent multifeature detectors.

The complex time series received by the radar in a certain range cell is $\mathbf{x} = \{x(n)|n = 1, 2, \ldots, N\}$. The TF transformation of the series is carried out by using the smooth pseudo Wigner–Ville distribution (SPWVD)

$$\mathrm{SPWVD}(n, l|\mathbf{x}) = \sum_{m=-M}^{M} g(m) \sum_{k=-K}^{K} h(k)$$
$$x(n+m+k)x^*(n+m-k)exp(-j4\pi kl\Delta f_d). \tag{13}$$

In (13), $g(m)$ and $h(k)$ are time and frequency smoothing windows, respectively. The superscript "*" indicates the conjugation of x, and Δf_d is sampling interval of the normalized Doppler frequency. Every TF image is normalized by the mean function and standard deviation function of the RCs, and then the ridge integration (RI) feature [30] is extracted from the normalized SPWVD

$$\mathrm{RI}(\mathbf{x}) \equiv \sum_{n=1}^{N} \Re(n, \mathrm{Ridge}(n|\mathbf{x})). \tag{14}$$

The $\Re$ is the normalized SPWVD TF image of returns, and the ridge of TF image is defined as $\mathrm{Ridge}(n|\mathbf{x}) = \arg\max_l\{\Re(n, l|\mathbf{x})\}$.

In the binary image of SPWVD, the connected region is defined as a set of pixels with a value of 1. According to the 4-connected criterion, a connected region set $\{\Omega_1, \Omega_2, \ldots, \Omega_W\}$ can be obtained from the binary image. The number of regions (NR) and the maximum size (MS) of connected regions features are extracted from the normalized SPWVD binary image

$$\mathrm{NR}(\mathbf{x}) \equiv W \tag{15}$$

$$\mathrm{MS}(\mathbf{x}) \equiv \max_{k=1,2,\ldots,W}\{\#\Omega_k\}. \tag{16}$$

Here, the histogram contrast of sea clutter and returns with target of eight features are shown in Fig. 2. As is shown, the eight detection features are different in the separation and distribution of the target and sea clutter, which roughly describes the detection ability of each detection feature. Moreover, the abovementioned eight detection features could reflect the differences between sea clutter and small target returns from different perspectives. Although the contribution provided by the correlated features is relatively small, it also has a benefit for the improvements in detection performance. Moreover, the isolation forest algorithm works well with a large number of uncorrelated features [25]. Therefore, we use the isolation forest algorithm to design a multifeature detector in this article.

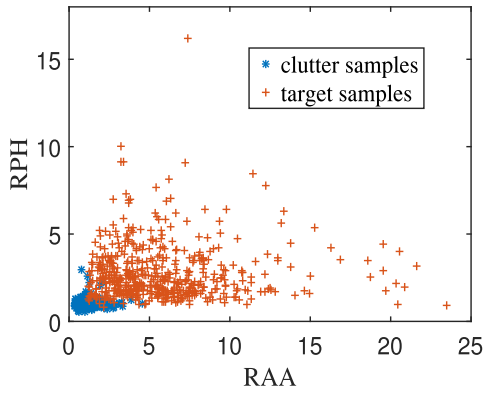

Fig. 3. Distribution of clutter samples and target samples on RAA and RPH plane.

B. Introduction of iForest Algorithm for Floating Small Target Detection

The binary hypothesis test for target detection can be regarded as a classification problem. Because of the difficulty of obtaining target returns and the diversity of targets, radar target detection is a typical one-class classification rather than a two-class classification problem. Therefore, a large number of classification methods need to get two kinds of samples to train the classifier [12], [17], but in the problem we need to solve, this condition is obviously not satisfied. But anomaly detection algorithms of machine learning can be utilized [20], [25], especially for the feature-based detection methods. In this way, sea clutter feature extracted from prereceived radar returns are regarded as normal samples and used to build anomaly detection model. On the contrary, the target feature samples are regarded as abnormal samples. Because the 2-D plane is more intuitive, we take the feature samples from RPH and RAA as an example. Fig. 3 illustrates the distribution of sea clutter samples and target samples on an RPH and RAA features 2-D plane. Fig. 4 illustrates the random partitioning of a target sample X_0 versus a sea-clutter sample X_1. The process is generated by randomly selecting a detection feature and randomly selecting a value between the minimum and maximum values of the selected feature. The sea clutter feature samples are recursively divided until all samples occupy a subspace by itself. Fig. 5 shows that sample X_0 far from other samples needs a small number of partitions, and it corresponds to the high SCR situation. However, the sample

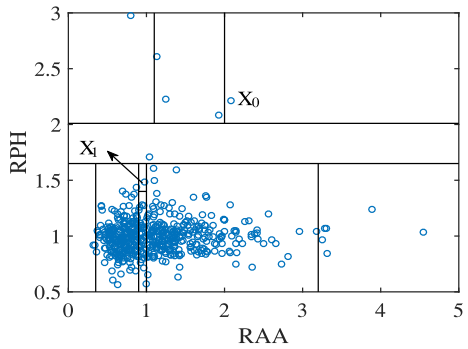

Fig. 4. Random partitioning of sea clutter samples.

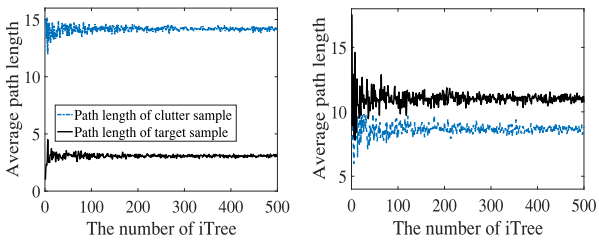

Fig. 5. Relationship between average path length and the number of iTree. (a) SCR is 8.252dB. (b) SCR is -0.219dB.

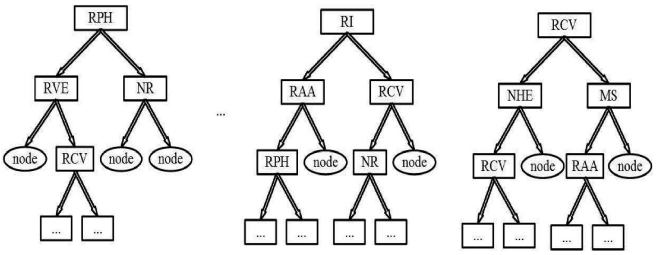

Fig. 6. Schematic diagram of iForest with the eight features.

X_1 near the center of the clutter samples requires much more partitions to isolate, which corresponds to the low SCR situation. Recursive partitioning of the feature space can be described by a *proper binary tree*, which is named as isolation Tree (iTree). Each leaf node of the binary tree corresponds to a feature subspace. Because of the random selection of features and feature values, a lot of binary trees can be created to improve the stability of detection. An iForest for floating small target detection is constructed and its sketch is shown in Fig. 6. Since the features of each node are randomly selected, Fig. 6 is a schematic diagram that is only a possible situation. Each node in Fig. 6 represents that the leaf node occupies a feature subspace alone. And it should be noted that features can be selected repeatedly in the same iTree.

C. Multifeature Detector Based on iForest and Its PFA's Adjustment

Based on iForest algorithm, the average path length of feature sample is used as the detection statistics instead of the calculation of anomaly score in the iForest. Moreover, the multifeature detector with adjustable PFA is realized. Since the target-plus-clutter samples are far away from the sea clutter samples compared with the other sea clutter samples, these samples are closer to the root node in every iTree, while most of the sea clutter samples are located at the deeper leaf nodes. Usually, the path lengths of sea clutter samples are greater than that of target samples. Thus the average path length of feature samples in an iForest can be used as the test statistic. Next, we will discuss the PFA adjustment for the iForest-based detector in the following part.

For the practical available detectors, a requisite property is that the PFA of the detectors is controllable. The multiple features of sea clutter obey the unknown parameter conditional probability density function (PDF), corresponding to a region in high-dimensional feature space. However, the complex multiple dimension conditional distribution and the limitation of target samples make the accurate probability model description infeasible. So the anomaly detection algorithm is an effective substitution for the joint PDF of clutter features. In our problem, the modified iForest algorithm is used to illustrate the conditional distribution of clutter features. We could acquire a region that only contains clutter features with the iForest algorithm. It takes the normal samples in a small region capturing most samples and anomaly samples elsewhere, which are corresponding to sea clutter samples and all kinds of target samples, respectively.

Another problem is that the detection decision region could be zoomed to adjust the PFA. We assume that the two conditional PDFs ($f(\boldsymbol{\zeta}|\mathrm{H}_0)$ and $f(\boldsymbol{\zeta}|\mathrm{H}_1)$, where $\boldsymbol{\zeta} = \{\boldsymbol{\xi}_1, \boldsymbol{\xi}_2, \ldots, \boldsymbol{\xi}_i, \ldots, \boldsymbol{\xi}_n\}$ is the feature sets, and $\boldsymbol{\xi}_i$ is a feature sample) are known. Under the guidance of Neyman–Person criterion, the decision region Ω could be obtained at the given PFA

$$\max_{\Omega}\{P_d = 1 - \int \cdots \int_{\Omega} f(\boldsymbol{\zeta}|\mathrm{H}_1)\,\mathrm{d}\boldsymbol{\zeta}\}$$
$$\text{s.t.} \int \cdots \int_{\Omega} f(\boldsymbol{\zeta}|\mathrm{H}_0)\,\mathrm{d}\boldsymbol{\zeta} = 1 - P_f \tag{17}$$

where P_d is the probability of detection and P_f is the PFA. However, it is unavailable to get the detection statistic because of the complexity of $f(\boldsymbol{\zeta}|\mathrm{H}_0)$ and the diversity of $f(\boldsymbol{\zeta}|\mathrm{H}_1)$. According to the geometric probability model, the probability can be approximated as the ratio of the number of feature samples in an area to the whole sample number. So the problem could be briefly described as

$$\max_{\Omega}\left\{P_d = \frac{\#\{\Xi - \Omega\}}{\#\{\Xi\}}, \quad \text{under } \mathrm{H}_1\right\}$$
$$\text{s.t.} \quad 1 - \frac{\#\{\Omega\}}{\#\{\Xi\}} \leqslant P_f, \quad \text{under } \mathrm{H}_0 \tag{18}$$

where Ξ is a detection region formed by the range of all features, and $\#\{\cdot\}$ indicates the number of the feature samples located in the region $\{\cdot\}$. So $\frac{\#\{\Omega\}}{\#\{\Xi\}}$ is the probability that the feature samples are inside the detection decision region under H_0 and $\frac{\#\{\Xi-\Omega\}}{\#\{\Xi\}}$ is the P_d that feature samples are outside the detection region under H_1.

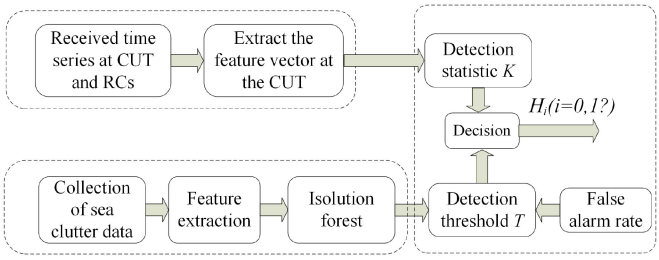

Fig. 7. Flowchart of the proposed iForest-based detector.

For the iForest-based detectors, the short average path length of target means that the PDF of signal features deviates from the PDF of clutter features, indicating that it is easy to be isolated. So under the H_0, the iForest-based detector can adjust the size of the detection decision region Ω by discarding some samples which are greatly deviated from the PDF of clutter to meet the PFA requirement. The procedure means that the detection region of the proposed detector is suitable for all targets while the SVM-based detector[17] is only optimal to the training target samples.

The iForest-based detector for floating small target detection controls the PFA by sorting all samples' average path length in ascending order and selecting a specific average path length as the detection threshold. It consists of two stages and the flowchart of the proposed iForest-based detector is shown in Fig. 7.

1) *Training stage*: In this stage, an iForest is built and the detection threshold is obtained via the widely used Monte-Carlo method. Constructing a sea clutter feature set $\boldsymbol{\zeta} = \{\boldsymbol{\xi}_1, \boldsymbol{\xi}_2, \ldots, \boldsymbol{\xi}_i, \ldots, \boldsymbol{\xi}_n\}$, which is extracted from prereceiving sea clutter returns and $\boldsymbol{\xi}_i = [\mathrm{NHE}(\mathbf{c}_i), \mathrm{RAA}(\mathbf{c}_i), \mathrm{RPH}(\mathbf{c}_i), \mathrm{RVE}(\mathbf{c}_i), \mathrm{RI}(\mathbf{c}_i), \mathrm{MS}(\mathbf{c}_i), \mathrm{NR}(\mathbf{c}_i), \mathrm{RCV}(\mathbf{c}_i)]^T$ denotes the ith sea clutter feature sample. Then, an iForest using the clutter feature set is built. Finally, the detection threshold is obtained according to Algorithm 1, which gives a detailed description of the process of the Monte-Carlo method to estimate the detection threshold. Average path length set is denoted as $L = \{l_1, l_2, \ldots, l_i, \ldots, l_N\}$, of which every average path length is acquired by iForest model as the sea clutter feature sample input. And it should be noted that the average path length set is sorted in ascending order. Therefore, the final detection threshold can be obtained by the number of false alarm. As a rule of thumb, the minimum value of N used in a detection radar signal simulation should be 10/PFA.

2) *Detection Stage*: In this stage, the eight features from the CUT returns are extracted and its average path length L_{CUT} is calculated by the iForest. After obtaining the average path length of CUT returns, the detection decision can be made by comparing the average path length of CUT L_{CUT} with the detection threshold T, which is shown as

$$L_{\mathrm{CUT}} \underset{\mathrm{H_1}}{\overset{\mathrm{H_0}}{\gtrless}} T. \tag{19}$$

It should be noted that the H_0 is selected when the L_{CUT} is greater than the decision threshold, and H_1 is selected when the L_{CUT} is less than the decision threshold.

Algorithm 1: Calculating Threshold Based on Monte-Carlo Method.

Inputs: $\boldsymbol{\zeta}$ - sea clutter feature set, $iForest$ - iForest Model,
P_f - PFA.
Output: T - detection threshold.

Initialize Set $N = \mathrm{size}(\boldsymbol{\zeta})$
  Set the number of false alarm $k = \mathrm{ceil}(N \times P_f)$
  Set average path length set $L = \mathrm{NULL}$
for $i = 1$ to N **do**
  $l_i \leftarrow iForest(\boldsymbol{\xi}_i), \boldsymbol{\xi}_i \in \boldsymbol{\zeta}$
  $L \leftarrow L \cup l_i$
end for
$L' = \mathrm{sort}(L)$ in ascending order
Obtain the detection threshold $T = L'_k$
return T

IV. Experimental Result and Performance Comparison

In this section, the twenty measured IPIX datasets shown in Table I are used to evaluate detection performance of the proposed detector. Here, we compare the iForest-based detector with some classical anomaly detection algorithms. Frankly speaking, there are only a few detectors that can obtain fair detection performance on IPIX datasets at present. Therefore, the proposed detector is compared with some existing detectors that have been successfully employed in floating small target detection.

In our experiments, the measured IPIX datasets are divided into two groups. One group extracted from RCs is used for training the detection model and the other extracted from CUT is used for detection performance validation. For every dataset, the length of observation vectors are set as 512 and 1024, corresponding to 0.512 and 1.024 s observation time length. In our experiments, the lowest PFA is set as 0.001. To acquire the stable detection decision threshold or region, short vectors are generated by a sliding window of length 512 or 1024 on every range cell with sliding interval 128. Therefore, more than 10 000 clutter feature samples and 1000 target feature samples for a dataset can be obtained.

First, we analyze the influence of the number of trials on the stability of the detection threshold estimation. Here the number of trials is equivalent to the number of feature samples from pure clutter. The result of binary hypothesis test of radar target detection can be expressed by binomial distribution [31]. According to the famous De Moivre–Laplace theorem, the binomial distribution can be approximated by the Gaussian distribution when the number of trials is large enough. In the experiment shown in Fig. 8, the error of detection threshold is quantitatively analyzed by Gaussian distribution. Fig. 8 shows the confidence interval of PFA versus the number of trials when PFA is 0.01 and 0.001, respectively. And the confidence level is 90%. The dotted line is the upper limits of the confidence interval, the solid line is the lower limits of the confidence interval, and the number of trials on the abscissa is normalized by the PFA. It can be seen from the figure that as the number of trials

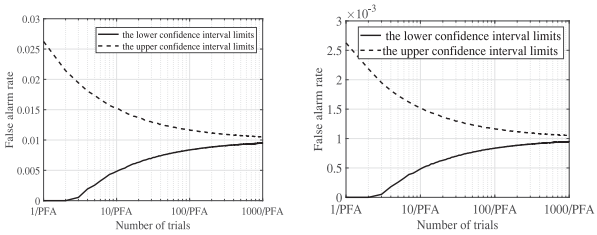

Fig. 8. Confidence limits (90 percent) on estimated PFA versus the number of trials. (a) PFA = 0.01. (b) PFA = 0.001.

increases, the confidence interval gradually decreases. In [31], the author stated that the minimum value of trials' number used in a detection radar signal simulation should be 10/PFA, and a value closer to 100/PFA is preferable. Therefore, in following experiments, 10 000 trials are used to estimate the detection threshold corresponding to PFA = 0.001 or a higher PFA.

The multifeature detector based on iForest has two parameters, the number of iTree N and the subsampling size K, which should be determined in advance. Here, we select a appropriate number of iTree by measuring the fluctuation of the average path length of clutter samples. Under different SCR cases, the fluctuation degree of the average path length in the range of different number of iTree is different, corresponding to different sea surface environmental conditions. So, the number of iTree could adapt to the sea clutter. Due to the lack of target samples in the detection, the appropriate number of iTree can only be determined according to the fluctuation degree of the average path length of sea clutter samples. From Fig. 5, we can see that the fluctuation trend of the average path length of the target sample is roughly similar to that of the sea clutter sample. In the experiment, the number of iTrees ranges from 1 to 500. The curve of the average path length of sea clutter with the number of iTree is shown in Fig. 5. Standard deviation is used to measure the fluctuation of the average path length in a certain range of the number of iTree. The average path length of sea clutter with different number of iTree is denoted as $a_1, a_2, \cdots, a_M$, M is the number of iTree. The window length is set as $W = 10$ and the sliding length of step is $step = 2$, the index set I of the average path length in data window i is expressed as

$$I = i \times step - 1 : i \times step + W - 2. \tag{20}$$

So we can get the standard deviation of the average path length in each window.

Fig. 9 shows the standard deviation versus the index of window for the clutter sample in Fig. 5(a). When the index of window is greater than 100, the fluctuations of standard deviation tend to stabilize. When the standard deviation in a window is less than the mean of the standard deviation in all windows, the number of iTrees corresponding to the median in the window is taken as the size of iForest. Therefore, each dataset will adaptively select the number of iTree based on the fluctuation of the average path length of sea clutter samples.

As for the subsampling size, Fig. 10 has plotted the relationship between average path length, probability of detection

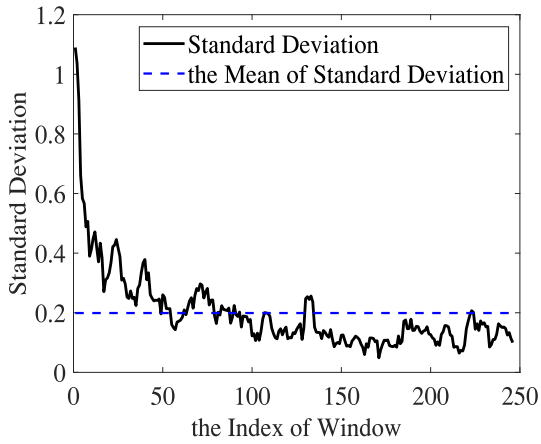

Fig. 9. Standard deviation versus the index of window for the clutter sample in Fig. 5(a).

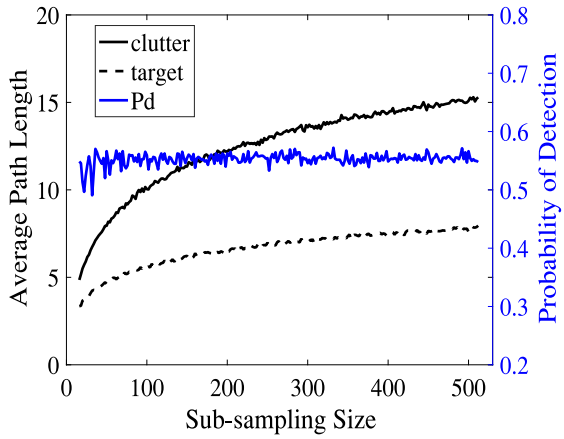

Fig. 10. Relationship between average path length, Pd and subsampling size, where average path length corresponds to left y-axis and Pd corresponds to right y-axis.

and subsampling size when the PFA is 0.001. As the subsampling size increases, the difference of the average path length between target samples and clutter samples becomes larger and larger. The detection probability fluctuates heavily when the subsampling size is less than about 100 while the probability of detection always fluctuates slightly around 0.55 when the interval is larger than 100. Moreover, the paper [25] has given an elaborate illustration that enough information for anomaly detection is provided when subsampling size $K = 256$. Therefore, considering the stability of detection, the subsampling size is set as 256, which is used as the default value in the following experiments.

A. Comparison Between iForest-Based Detector and Other Anomaly Detectors

There are lots of anomaly detection algorithms in machine learning, however, some of them lose effectiveness when they are employed in radar target detection because of the rigorous steerable PFA requirement under the Neyman–Pearson criterion. For example, robust covariance cannot acquire a proper test

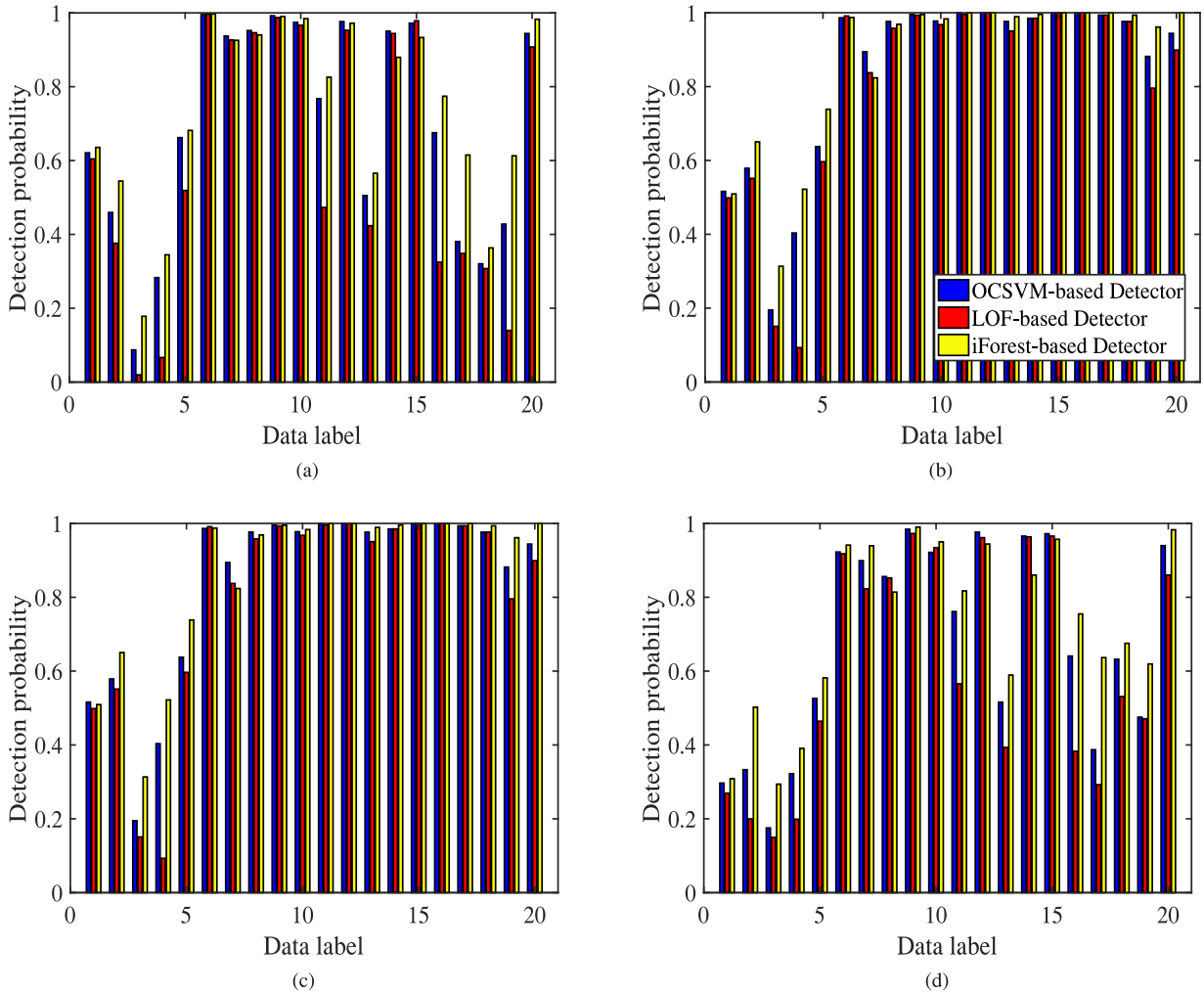

Fig. 11. Detection probability histogram of the OCSVM-based detector, the LOF detector and the iForest-based detector when observation time is 0.512 s and the PFA is 0.001. (a) HH. (b) HV. (c) VH. (d) VV polarizations.

statistic, let alone the PFA. Here, we compare the iForest-based detector with the LOF-based detector and the OCSVM-based detector. The LOF-based algorithm could measure the local density of feature distribution, and the reciprocal transformation of local density is defined as an outlier factor. So the LOF can be used as the test statistic straightly. The OCSVM-based detector constructs the decision region in high-dimensional feature space under the guidance of the PFA to distinguish target and clutter. In this experiment, the PFA is set as 0.001 and the observation time is set as 0.512 s. Fig. 11 shows the detection probability of the LOF-based detector, the OCSVM-based detector, and the iForest-based detector. There are two conclusions that be drawn from Fig. 11.

1) The detection performance of the three anomaly detectors under cross-polarization is better than that under the like-polarization. It is mainly caused by the difference of sea-surface's scattering mechanism at the different polarizations, and data collecting with cross-polarizations have higher ASCR than that with like-polarizations.

2) Figs. 1 and 11 indicate that the iForest-based detector is superior to the LOF-based detector and the OCSVM-based detector in the datasets with low ASCR and all of the three detectors have excellent detection performances in the datasets with high ASCR.

The three detectors have employed all eight features, and they could construct different detection regions according to their anomaly detection criterion. From Fig. 11, we can see that the three anomaly detectors have good detection performances in the case of high ASCR. But in the case of low ASCR, the multifeature detector based on iForest has an absolutely better detection performance. This is mainly due to the difference of the detection decision regions created by different detection algorithms according to PFA. Fig. 12 is a schematic diagram of the 2-D detection decision regions of the three anomaly detectors when the PFA is 0.1. The number of training samples is 240, where 216 samples obey the Gaussian distribution with mean value of 0, variance of 0.1, and correlation coefficient of 0. Then, 24 abnormal samples obey the uniform distribution in $[-6, 6]$. Fig. 12 indicates that the iForest algorithm can form a nonconvex detection region and reduce the detection region in a specific direction, which is the key to improving the detection performance. In general, the detection performance of

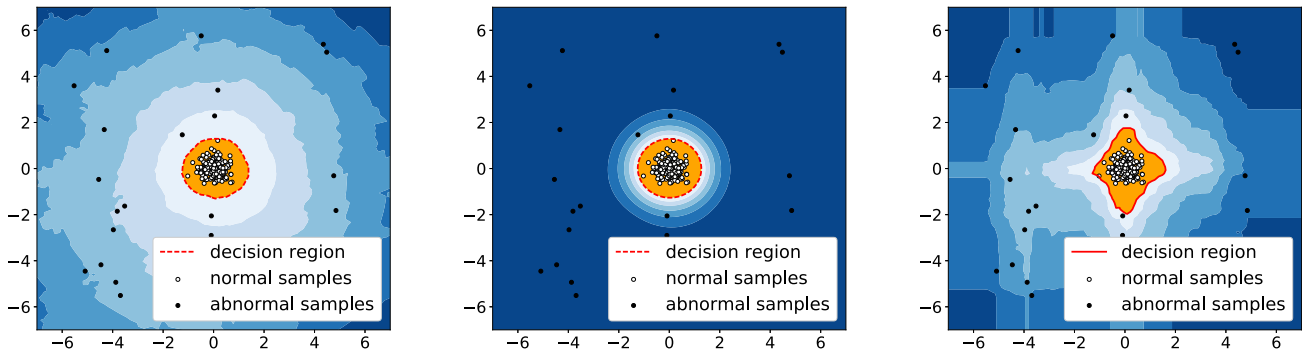

Fig. 12. Decision region schematic diagram. (a) LOF-based detector. (b) OCSVM-based detector. (c) iForest-based detector.

TABLE II
AVERAGE DETECTION PROBABILITIES OF THE FOUR DETECTORS ON THE TWENTY DATASETS AT EACH POLARIZATION

Observation time(s)	0.512				1.024			
Polarizations	HH	HV	VH	VV	HH	HV	VH	VV
NHE detector	0.223	0.404	0.448	0.241	0.301	0.536	0.576	0.328
Tri-feature-based detector	0.577	0.736	0.776	0.569	0.622	0.797	0.813	0.589
Time-Frequency detector	0.747	0.826	0.824	0.706	**0.821**	0.882	0.878	0.789
Proposed detector	**0.749**	**0.870**	**0.877**	**0.739**	0.819	**0.909**	**0.900**	**0.812**

the iForest-based detector is better and the detection stability is higher especially for floating small target detection.

B. Comparison Between iForest-Based Detector and Classical Detectors

In the second experiment, the iForest-based detector is compared with the normalized Hurst exponent (NHE) detector [10], the trifeature-based detector [14], and the TF features detector [16]. For the observation time 0.512 and 1.024 s, Table II has listed the four detectors' average probability of detection on twenty datasets when PFA is 0.001. In Table II, the best detection probabilities for each polarization in two different observation times are denoted by the bold entities. According to Table II, the proposed detector acquires the best detection performance among the four detectors on average, except for HH polarization with the observation time is 1.024 s. The multifeature detector based on iForest could catch much more differences between target and sea clutter because it consists of all the other detectors' features. As for HH polarization, the TF features play a predominant role in the iFoest-based detector and the description of iForest's decision region is not finer than convexhull-class detector. So the iForest-based detector shows some performance loss in the case of some features with poor separating capacity. It is worth nothing that the computational complexity of convexhull-class detector is $O(LN^2\log(K))$, where L is the number of abandoned samples to guarantee the PFA requirement and K is the number of convexhull's vertexes. Benefiting from the advantages of the iForest algorithm, the iForest-based detector has the linear time complexity, where $O(NK\log K)$ is for training stage and $O(SN\log K)$ is for detection stage, where N is the number of iTree, K is the subsampling for constructing every iTree and

TABLE III
ELAPSED TIME FOR BUILDING DETECTION MODELS

Detector	PFA		
	0.001	0.01	0.1
Convexhull-class detector	16.541s	163.208s	2385.7s
Proposed detector	14.945s	15.694s	15.741s

S is the detection data size. For the complex and changeable sea-surface background, the key to realizing the real-time detection is the fast extraction of detection features and the fast construction of detection model. Owing to the amount of data needed for each detection is relatively small, it is easy to achieve the fast extraction of detection features. In order to adapt to the change of sea-surface background, the rapid construction of detection model is the key factor that restricts the application. Table III shows the elapsed time of building a detection model under a given PFA. The elapsed time of building a convexhull-class model is related to the sample size and PFA. When the number of samples is fixed (it is 10 000 here), the elapsed time of the convexhull-class detector increases with the increase of PFA. However, when the amount of training samples is large, it will take a lot of time to create a convexhull model though the PFA is low. The linear computational complexity of the iForest-based detector is much lower than that of the convexhull-class detector and it is only related to the amount of training samples when the model parameters are given. The determination of detection decision region is only to select a suitable threshold from the ordered average path length. Theoretical analysis and experimental verification show that the computational complexity of the iForest-based detector is much less than that of convexhull-class detector, so it relatively

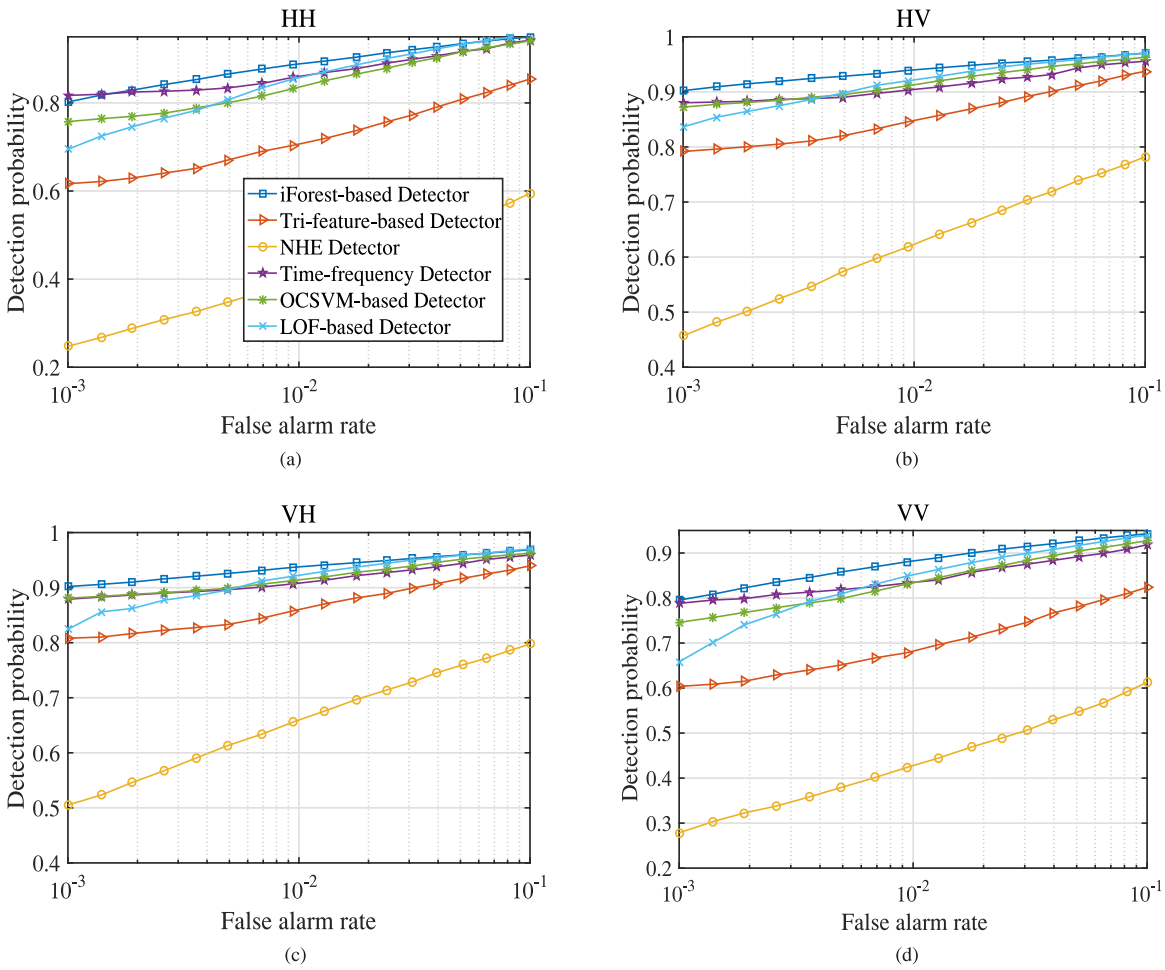

Fig. 13. Comparisons of the receiver operation characteristic (ROC) curves at (a) HH, (b) HV, (c) VH, and (d) VV polarizations when the observation time for a test is 1.024 s.

adapt to the complex and changeable sea-surface background for fast feature extraction and detector construction.

Then, the receiver operation curves (ROC) of the proposed detector and the other detectors at four polarizations are illustrated in Fig. 13. Here, the length of time series is set as 1024, and the PFA ranges from 0.001 to 0.1. The proposed detector obtains the best detection performance. The normalized Hurst exponent has a great detection performance loss. Compared with the LOF-based detector and the OCSVM-based detector, the iForest-based detector shows good robustness. Although the TF detector holds an acceptable performance loss compared with the proposed detector, its computational complexity is too high. In conclusion, the iForest-based detector is an effective multiple features detector and also has a low computation cost.

V. Conclusion

In this article, the proposed relative Doppler coefficient of variation detection feature and the multifeature detector based on modified isolation forest algorithm are used to expand the number of detection features and realize joint detection of multiple features, respectively. Via modifying the original iForest algorithm, the average path length is used as the detection statistic that could easily control the false alarm probability. Compared with some anomaly-detection-based detector and several existing detectors, the multifeature detector based on iForest shows the excellent performance especially in low ASCR case, and with low computational complexity.

The proposed detector breaks through the limitation of the number of features and realizes the high-performance floating small target detection under the controllable PFA. Therefore, our work is applicable to the detection of small targets on the sea surface by shore-based radar. Limited by the size of available dataset, the detection threshold obtained by Monte-Carlo method may slightly deviate from the corresponding preset PFA. According to the analysis, when the number of trials for Monte-Carlo experiments is large enough, the deviation can be tolerated. Moreover, the proposed iForest-based detector focuses on the innovation of multifeature combination algorithms in this article. The evaluation of different features will be researched in the future, and more features can also be explored to add into our proposed multifeature combination detection scheme.

REFERENCES

[1] T. J. Nohara and S. Haykin, "AR-based growler detection in sea clutter," *IEEE Trans. Signal Proc.*, vol. 41, no. 3, pp. 1259–1271, Mar. 1993.

[2] T. J. Nohara and S. Haykin, "Growler detection in sea clutter with coherent radars," *IEEE Trans. Aerosp. Electron. Syst.*, vol. 30, no. 3, pp. 836–847, Jul. 1994.

[3] K. D. Ward, "Compound representation of high resolution sea clutter," *Electron. Lett.*, vol. 17, no. 16, pp. 561—563 563, Aug. 1981.

[4] G. V. Weinberg, "Assessing Pareto fit to high-resolution high-grazing-angle sea clutter," *Electron. Lett.*, vol. 47, no. 8, pp. 516–517, Apr. 2011.

[5] K. J. Sangston, F. Gini, and M. S. Greco, "Coherent radar target detection in heavy-tailed compound-Gaussian clutter," *IEEE Trans. Aerosp. Electron. Syst.*, vol. 48, no. 1, pp. 64–77, Jan. 2012.

[6] Y. C. Gao, G. S. Liao, and S. Q. Zhu, "Adaptive signal detection in compound-Gaussian clutter with inverse Gaussian texture," in *Proc. 14th Int. Radar Symp.*, 2013, pp. 935–940.

[7] E. Jay, J. P. Ovarlez, D. Declercq, and P. Duvaut, "Bayesian optimum radar detector in non-Gaussian noise," in *Proc. Int. Conf. Acoust., Speech, Signal Process.*, 2002, pp. II-1289–II-1292.

[8] S. Shi, P. Shui, M. Liu, and S. Xu, "Subband adaptive coherent detection of weak moving targets in K-distributed sea clutter," in *Proc. CIE Int. Conf. Radar*, pp. 1–4, Oct. 2016.

[9] P. Shui and Y. Shi, "Subband ANMF detection of moving targets in sea clutter," *IEEE Trans. Aerosp. Electron. Syst.*, vol. 48, no. 4, pp. 3578–3593, Oct. 2012.

[10] D. Li and P. Shui, "Floating small target detection in sea clutter via normalised hurst exponent," *Electron. Lett.*, vol. 50, no. 17, pp. 1240–1242, Aug. 2014.

[11] T. K. Bhattacharya and S. Haykin, "Neural network-based adaptive radar detection scheme for small ice targets in sea clutter," *Electron. Lett.*, vol. 28, no. 16, pp. 1528–1529, Jul. 1992.

[12] G. Lopez-Risueno, J. Grajal, and R. Diaz-Oliver, "Target detection in sea clutter using convolutional neural networks," in *Proc. IEEE Radar Conf.*, May 2003, pp. 321–328.

[13] M. Arnaudon, F. Barbaresco, and L. Yang, "Riemannian medians and means with applications to radar signal processing," *IEEE J. Sel. Top. Signal Proc.*, vol. 7, no. 4, pp. 595–604, Aug. 2013.

[14] P. Shui, D. Li, and S. Xu, "Tri-feature-based detection of floating small targets in sea clutter," *IEEE Trans. Aerosp. Electron. Syst.*, vol. 50, no. 2, pp. 1416–1430, Apr. 2014.

[15] S. Xu, J. Zheng, J. Pu, and P. Shui, "Sea-surface floating small target detection based on polarization features," *IEEE Geosci. Remote Sens. Lett.*, vol. 15, no. 10, pp. 1505–1509, Oct. 2018.

[16] S. Shi and P. Shui, "Sea-surface floating small target detection by one-class classifier in time-frequency feature space," *IEEE Trans. Geosci. Remote Sens.*, vol. 56, no. 11, pp. 6395–6411, Nov. 2018.

[17] Y. Li, P. Xie, Z. Tang, T. Jiang, and P. Qi, "SVM-based sea-surface small target detection: A false-alarm-rate-controllable approach," *IEEE Geosci. Remote Sens. Lett.*, vol. 16, no. 8, pp. 1225–1229, Aug. 2019.

[18] T. Gu, "Detection of small floating targets on the sea surface based on multi-features and principal component analysis," *IEEE Geosci. Remote Sens. Lett.*, vol. 17, no. 5, pp. 809–813, May 2020.

[19] V. Chandola, A. Banerjee, and V. Kumar, "Anomaly detection:A survey," *Acm Comput. Surv.*, vol. 41, no. 3, pp. 1–58, 2009.

[20] Z. Gan and X. Zhou, "Abnormal network traffic detection based on improved LOF algorithm," in *Proc. 10th Int. Conf. Intell. Human-Mach. Syst. Cybern.*, vol. 01, Aug. 2018, pp. 142–145.

[21] M. M. Breunig, "LOF: Identifying density-based local outliers," in *Proc. Acm Sigmod Int. Conf. Manage. Data*, 2000, pp. 93–104.

[22] L. M. Manevitz and M. Yousef, "One-class SVMs for document classification," *J. Mach. Learn. Res.*, vol. 2, no. 1, pp. 139–154, 2001.

[23] Y. Wang, J. Wong, and A. Miner, "Anomaly intrusion detection using one class SVM," in *Proc. Inf. Assurance Workshop, Proc. Fifth Annu. IEEE SMC Inf. Assurance Workshop*, 2004, pp. 358–364.

[24] R. A. Maronna and R. H. Zamar, "Robust estimates of location and dispersion for high-dimensional datasets," *Technometrics*, vol. 44, no. 4, pp. 307–317, 2002.

[25] F. T. Liu, K. M. Ting, and Z. Zhou, "Isolation forest," in *Proc. 8th IEEE Int. Conf. Data Mining*, Dec. 2008, pp. 413–422.

[26] S. Ahmed, Y. Lee, H. Seung-Ho, and I. Koo, "Unsupervised machine learning based detection of covert data integrity assault in smart grid networks utilizing isolation forest," *IEEE Trans. Inf. Forensics Secur.*, vol. 14, no. 10, pp. 2765–2777, Oct. 2019.

[27] The McMaster IPIX Radar Sea Clutter Database. Accessed: Jul. 1, 2001. [Online]. Available: http://soma.ece.mcmaster.ca/ipix/

[28] X. Wang, J. Liu, and H. Liu, "Small target detection in sea clutter based on Doppler spectrum features," in *Proc. CIE Int. Conf. Radar*, pp. 1–4, Oct. 2006.

[29] X. Yang, G. Wen, C. Ma, B. Hui, B. Ding, and Y. Zhang, "CFAR detection of moving range-spread target in white Gaussian noise using waveform contrast," *IEEE Geosci. Remote Sens. Lett.*, vol. 13, no. 2, pp. 282–286, Feb. 2016.

[30] P. Shui, Z. Bao, and H. Su, "Nonparametric detection of FM signals using time-frequency ridge energy," *IEEE Trans. Signal Proc.*, vol. 56, no. 5, pp. 1749–1760, May 2008.

[31] J. D. Echard, "Estimation of radar detection and false alarm probability," *IEEE Trans. Aerosp. Electron. Syst.*, vol. 27, no. 2, pp. 255–260, Mar. 1991.

Shuwen Xu (Member, IEEE) was born in Huangshan city in Anhui, China. He received the B.Eng. and Ph.D. degrees from Xidian University, Xian, China, in 2006 and 2011, respectively, both in electronic engineering.

He worked with the National Laboratory of Radar Signal Processing, Xidian University. From 2011, he worked as a Visiting Professor with Mcmaster University, Hamilton, ON, Canada, in 2018. He is currently a Professor and an Advisor of Ph..D. students with the National Laboratory of Radar Signal Processing, Xidian University. His research interests include radar target detection, statistical Learning, and SAR image processing.

Jianan Zhu was born in Jilin city in Jilin, China. He received the B.Eng. degree in detection, guidance, and control technology, and the M.S. degree in electronic engineering, both from Xidian University, Xian, China, in 2017 and 2020, respectively.

He works with Nanjing Research Institute of Electronics Technology, China. His research interests include radar target detection.

Junzheng Jiang received the B.S. degree in applied math from Guilin University of Electronic Technology, Guilin, China, in 2005, and the Ph.D. degree in information and communication engineering from Xidian University, Xian, China, in 2011.

Since 2011, he has been with the Guilin University of Electronic Technology, where he is currently a Full Professor and an Advisor of Ph.D. students. He was a Visiting Scholar with the University of Central Florida, USA, from February 2016 to February 2017. His research interests include graph filter bank, distributed signal processing on graphs, time-vertex signal processing on graphs.

Penglang Shui (Senior Member, IEEE) was born in Xi'an, China, in 1967. He received the B.S. degree in applied mathematics from Xidian University, Xi'an, China, in 1989, the M.S. degree in mathematics from Nanjing University, Nanjing, China, in 1992, and the Ph.D. degree in electrical engineering from Xidian University, in 1999.

He is currently a Professor with the National Laboratory of Radar Signal Processing, Xidian University. His research interests include multirate filter bank theory and applications, image processing, and radar target detection and tracking.